Supplement of Ocean Sci., 20, 1051–1066, 2024
https://doi.org/10.5194/os-20-1051-2024-supplement

Ocean Science Open Access EGU

Supplement of

The characteristics of tides and their effects on the general circulation of the Mediterranean Sea

Bethany McDonagh et al.

Correspondence to: Bethany McDonagh (bethany.mcdonagh@cmcc.it) and Emanuela Clementi (emanuela.clementi@cmcc.it)

S1 Preliminary experiments

As discussed in Section 2 and Table 2 of the manuscript, there are some differences between the two experiments which are not directly related to the implementation of tidal forcing. Some preliminary experiments were carried out to assess the impact of changing the timestep and time-stepping scheme, as was required for stability in the tidal experiment.

Figure S1 shows the differences in sea surface height and currents over a four-year experiment with a change in the time integration scheme. From this, we see that changes in sea surface height are on the order of 5 mm, and currents change on the order of 5×10^{-4} ms^{-1}. These are both negligible with respect to the changes due to tidal forcing. Changes in salinity (Fig. S2) are also negligible, on the order of 10^{-4} PSU, which is 10% of the magnitude of the changes due to tides (see Section 6 of the manuscript).

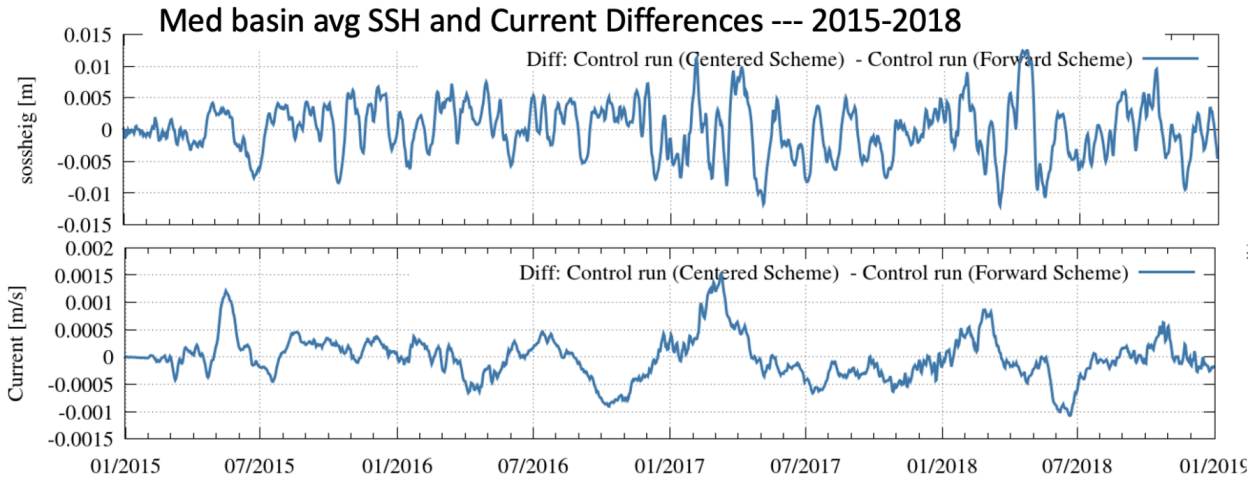

Figure S1: Differences between Mediterranean Sea average sea level (top) and currents (bottom), computed from control runs with forward and centred time integration schemes.

S2 The Gibraltar Strait

Mass transport at the Gibraltar Strait is affected by tides, as was shown by Gonzalez et al. (2023), Harzallah et al. (2014), and Naranjo et al. (2014). Net water mass transport through the strait at a given longitude, over the five-year period, was calculated as:

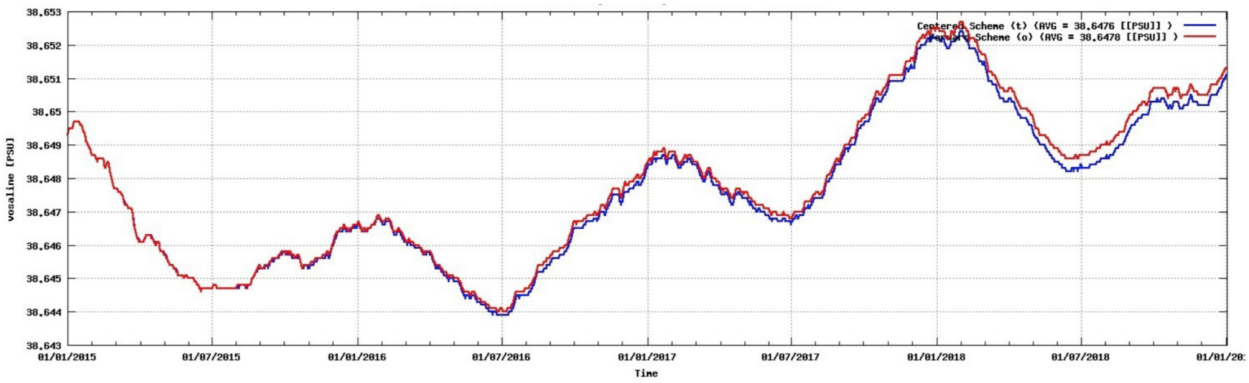

Figure S2: Time-series of Mediterranean Sea average salinity, computed from control runs with forward and centred time integration schemes. The centred time integration scheme is in blue and the forward scheme is in red.

$$\bar{Q}(x) = \int_{South}^{North} \int_{-d}^{\eta} \bar{u} dz dy \tag{1}$$

where $\bar{Q}$ is the net water mass transport, η is the sea surface height, $-d$ is the depth, and $\bar{u}$ is the mean zonal velocity. This transport can be split into eastward and westward components:

$$\bar{Q}_{in}(x) = \int_{South}^{North} \int_{-d}^{\eta} \bar{u} H(u) dz dy \tag{2}$$

$$\bar{Q}_{out}(x) = \int_{South}^{North} \int_{-d}^{\eta} \bar{u} H(-u) dz dy \tag{3}$$

where Q_{in} is the upper-layer eastward transport, Q_{out} is the lower-layer westward transport, and H is the Heaviside step function, $H = 1$ if $u > 0$, $H(u) = 0$ otherwise.

The effects of tides on the Gibraltar Strait mass transport are detailed in Table S1. Although the net transport in the Gibraltar Strait is not largely affected by tides, both the inflow and outflowing transport are increased by tides. Within observational errors we cannot fully distinguish between the tide and no-tide experiments, but we can estimate a 5-10% larger inflow/outflow transport with respect to literature. We argue that this is due to the relatively coarse resolution of the model in the Gibraltar Strait, since Sannino et al. (2009) demonstrated that the required resolution for an accurate representation of the Gibraltar

Experiment	Inflow ($\bar{Q}_{in}$)	Outflow ($\bar{Q}_{out}$)	Net Transport ($\bar{Q}$)
Model without tides	0.85 Sv	-0.80 Sv	0.045 Sv
Tidal model	0.88 Sv	-0.84 Sv	0.043 Sv
Observations (Soto-Navarro et al., 2010)	0.81$\pm$0.06 Sv	-0.78$\pm$0.05 Sv	0.038$\pm$0.007 Sv

Table S1: Mass transport at the 5.48°W section of the Gibraltar Strait in the experiment without tides, tidal experiment, and observations from Soto-Navarro et al. (2010). Values for model outputs are calculated as mean inflow and outflow transport in the Gibraltar Strait for the period 2017-2021.

Strait would be at the sub-kilometer scale, many times greater than the one used in our model.

S3 Spectra of additional regions

The kinetic energy analysis in Section 4 of the manuscript for three points (Gibraltar Strait, Tyrrhenian Sea, and Cretan Sea) are discussed, but six additional points were analysed, as shown in Fig. 1 of the manuscript. Figures equivalent to Figs. 5-9 in the manuscript, but for these six points, are presented here. The figures are organised alphabetically by region. Note that only barotropic spectra of the Gulf of Gabes and North Adriatic are shown, since the regions are shallow.

S3.1 Gulf of Gabes

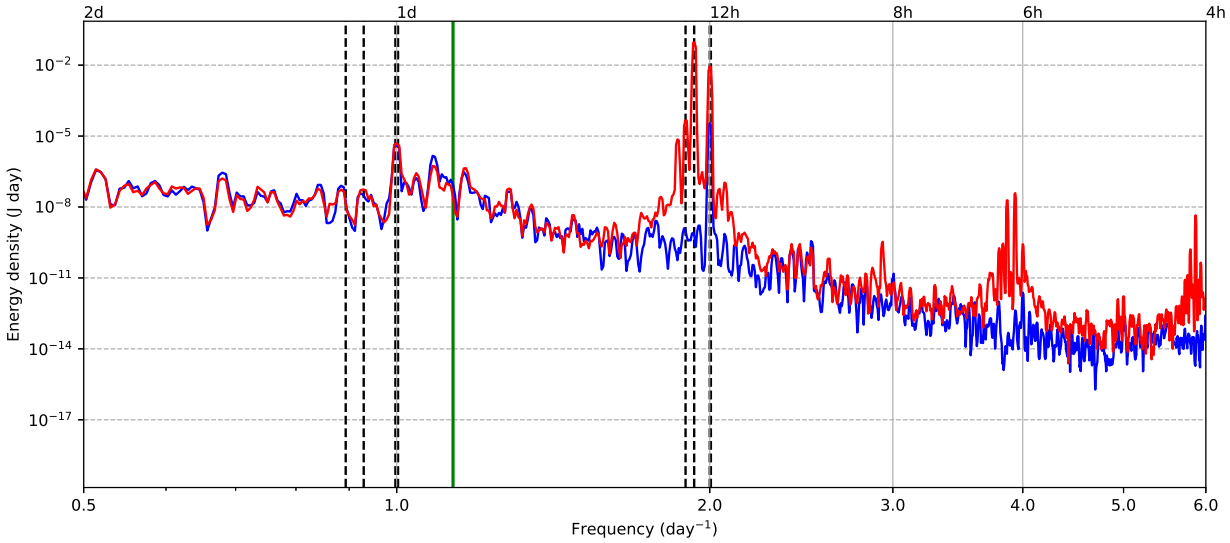

Figure S3: Barotropic rotary spectrum of kinetic energy density at the Gulf of Gabes point (34.52°N, 11.42°E), averaged across all depths, for a six-month period (January-June 2019). Dashed lines represent the eight tidal components included in the model, and the green line is the inertial frequency.

S3.2 Gulf of Lion

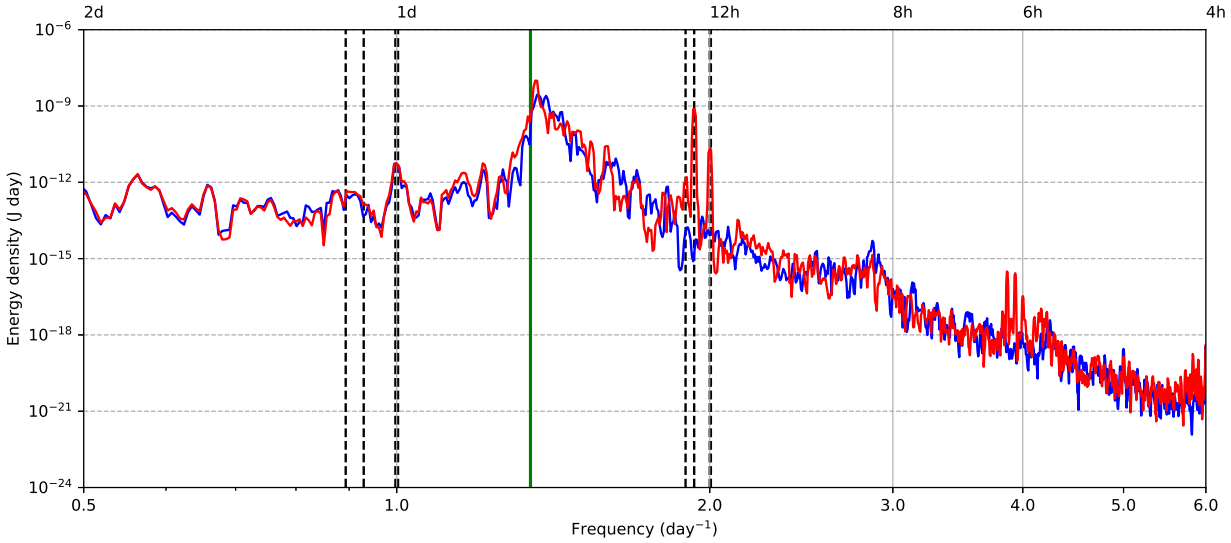

Figure S4: Barotropic rotary spectrum of kinetic energy density at the Gulf of Lion point (42.27°N, 5.25°E), averaged across all depths, for a six-month period (January-June 2019). Dashed lines represent the eight tidal components included in the model, and the green line is the inertial frequency.

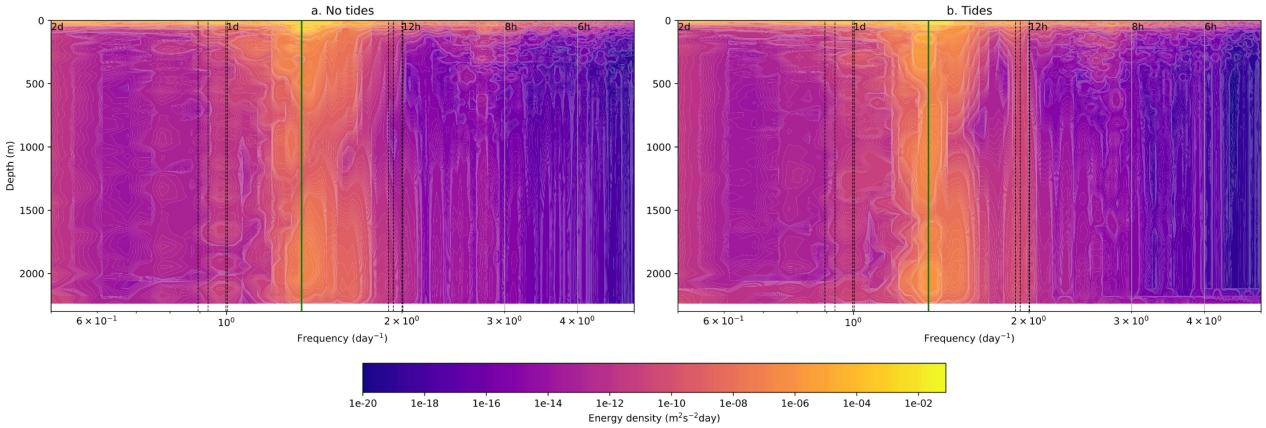

Figure S5: Rotary spectrum of kinetic energy density at the Gulf of Lion point (42.27°N, 5.25°E), for all depths, over a six-month period (January-June 2019). Dashed lines represent the eight tidal components included in the model, and the green line is the inertial frequency.

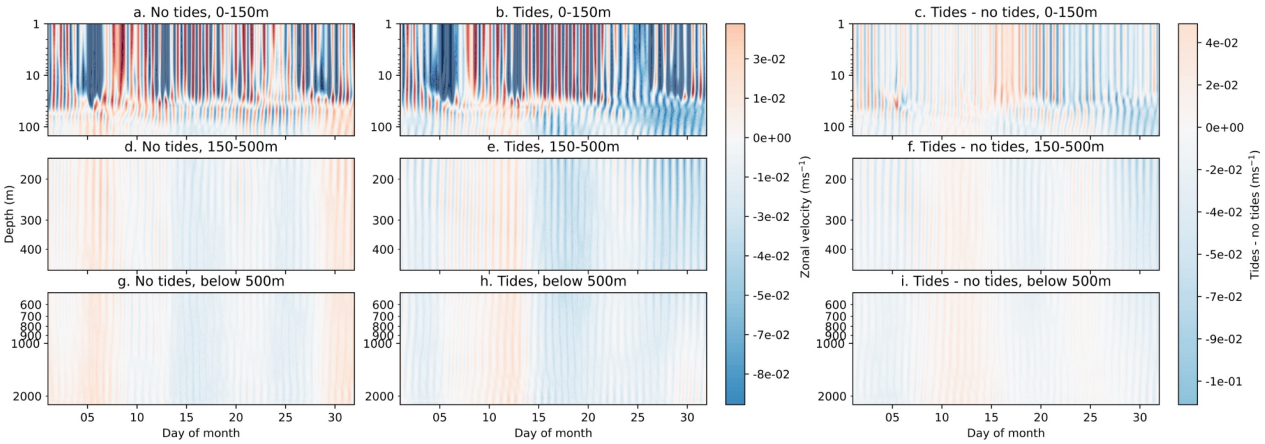

Figure S6: Hovmoller plots of depth against time of hourly mean zonal velocity at a point at the Gulf of Lion point (42.27°N, 5.25°E) in May 2019, for a. Model without tides, 0-150m, b. Tidal model, 0-150m, c. Tidal model – model without tides, 0-150m, d. Model without tides, 150-500m, e. Tidal model, 150-500m, f. Tidal model – model without tides, g. Model without tides, below 500m, h. Tidal model, below 500m, i. Tidal model – model without tides, below 500m. Note that the depth scale is logarithmic.

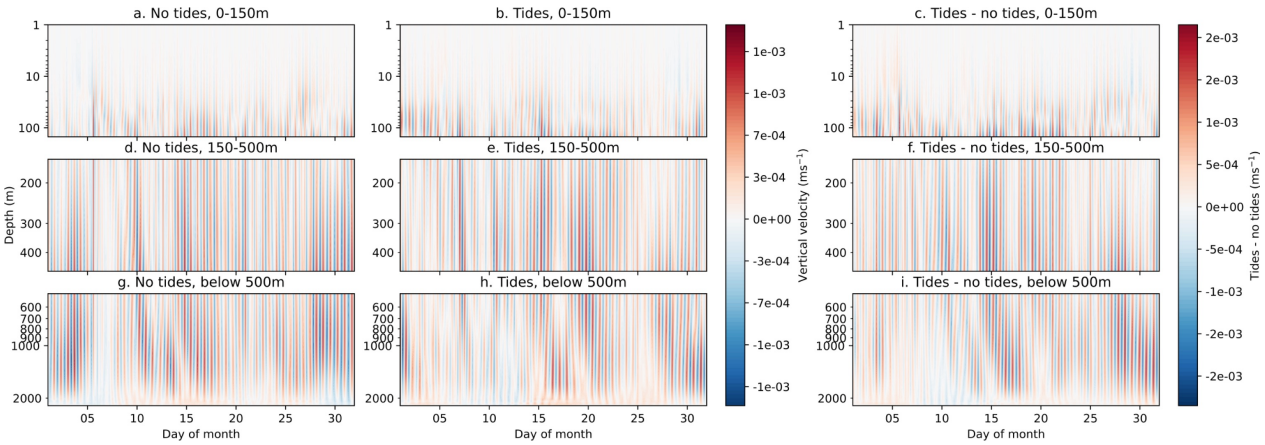

Figure S7: Hovmoller plots of depth against time of hourly mean vertical velocity at a point at the Gulf of Lion point (42.27°N, 5.25°E) in May 2019, for a. Model without tides, 0-150m, b. Tidal model, 0-150m, c. Tidal model – model without tides, 0-150m, d. Model without tides, 150-500m, e. Tidal model, 150-500m, f. Tidal model – model without tides, g. Model without tides, below 500m, h. Tidal model, below 500m, i. Tidal model – model without tides, below 500m. Note that the depth scale is logarithmic.

S3.3 Ionian Sea

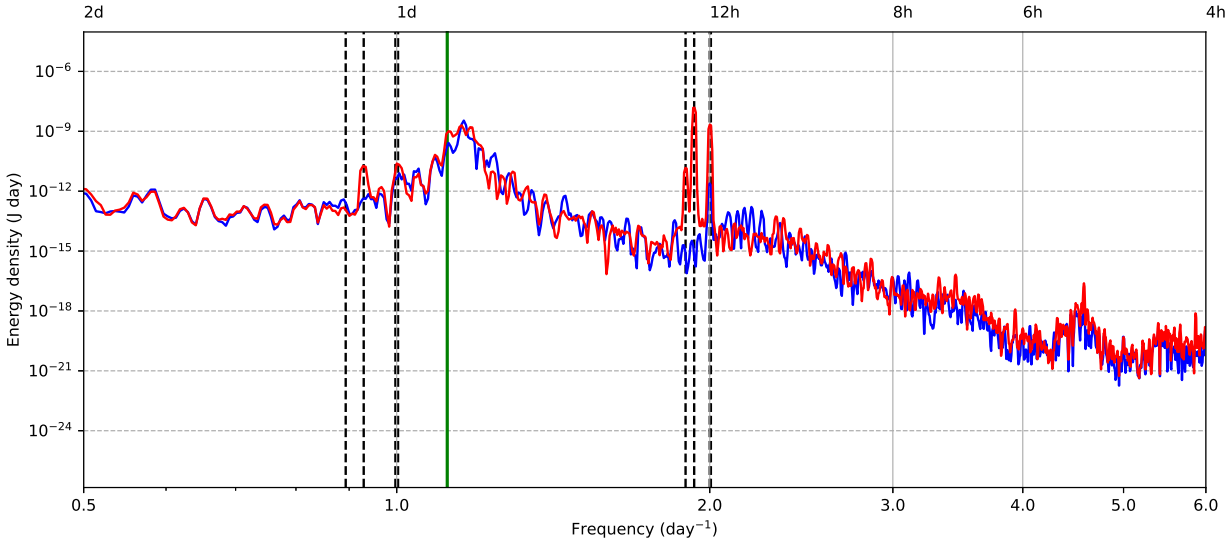

Figure S8: Barotropic rotary spectrum of kinetic energy density at the Ionian Sea point (34.02°N, 20.00°E), averaged across all depths, for a six-month period (January-June 2019). Dashed lines represent the eight tidal components included in the model, and the green line is the inertial frequency.

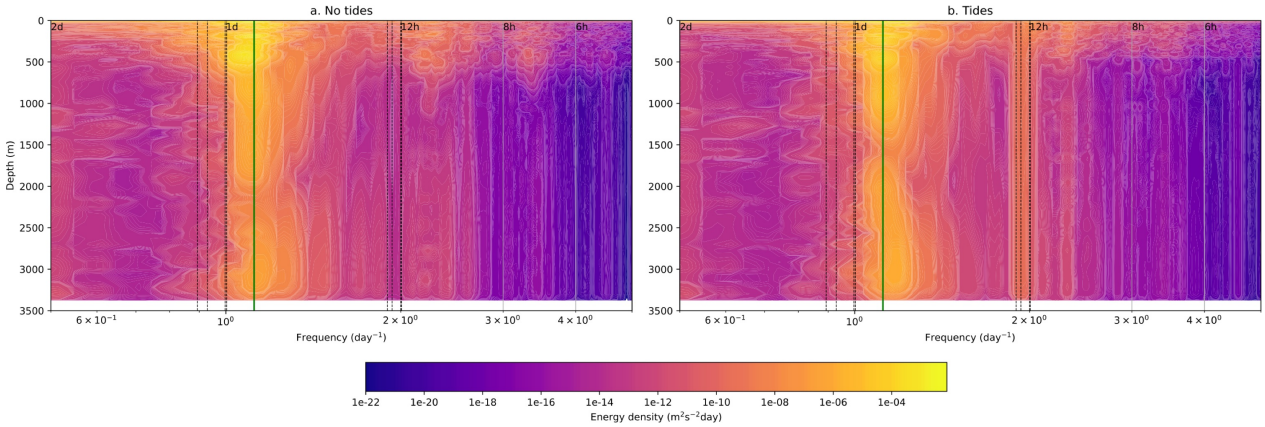

Figure S9: Rotary spectrum of kinetic energy density at the Ionian Sea point (34.02°N, 20.00°E), for all depths, over a six-month period (January-June 2019). Dashed lines represent the eight tidal components included in the model, and the green line is the inertial frequency.

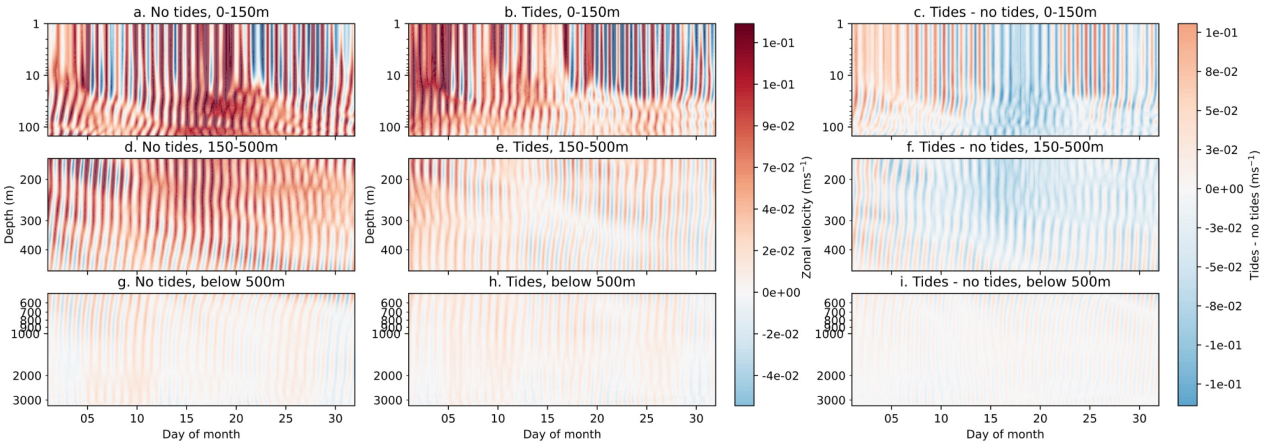

Figure S10: Hovmoller plots of depth against time of hourly mean zonal velocity at a point at the Ionian Sea point (34.02°N, 20.00°E) in May 2019, for a. Model without tides, 0-150m, b. Tidal model, 0-150m, c. Tidal model – model without tides, 0-150m, d. Model without tides, 150-500m, e. Tidal model, 150-500m, f. Tidal model – model without tides, g. Model without tides, below 500m, h. Tidal model, below 500m, i. Tidal model – model without tides, below 500m. Note that the depth scale is logarithmic.

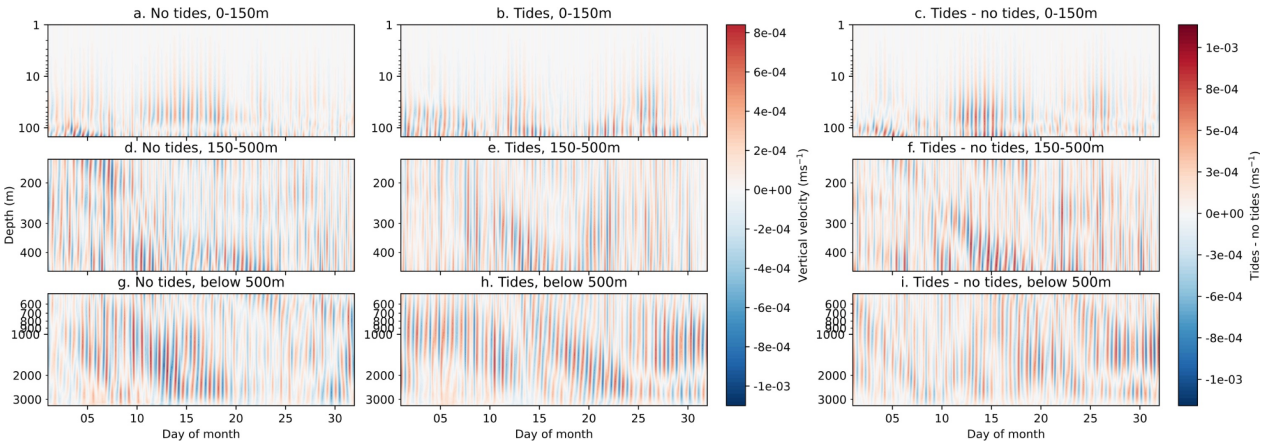

Figure S11: Hovmoller plots of depth against time of hourly mean vertical velocity at a point at the Ionian Sea point (34.02°N, 20.00°E) in May 2019, for a. Model without tides, 0-150m, b. Tidal model, 0-150m, c. Tidal model – model without tides, 0-150m, d. Model without tides, 150-500m, e. Tidal model, 150-500m, f. Tidal model – model without tides, g. Model without tides, below 500m, h. Tidal model, below 500m, i. Tidal model – model without tides, below 500m. Note that the depth scale is logarithmic.

S3.4 North Adriatic Sea

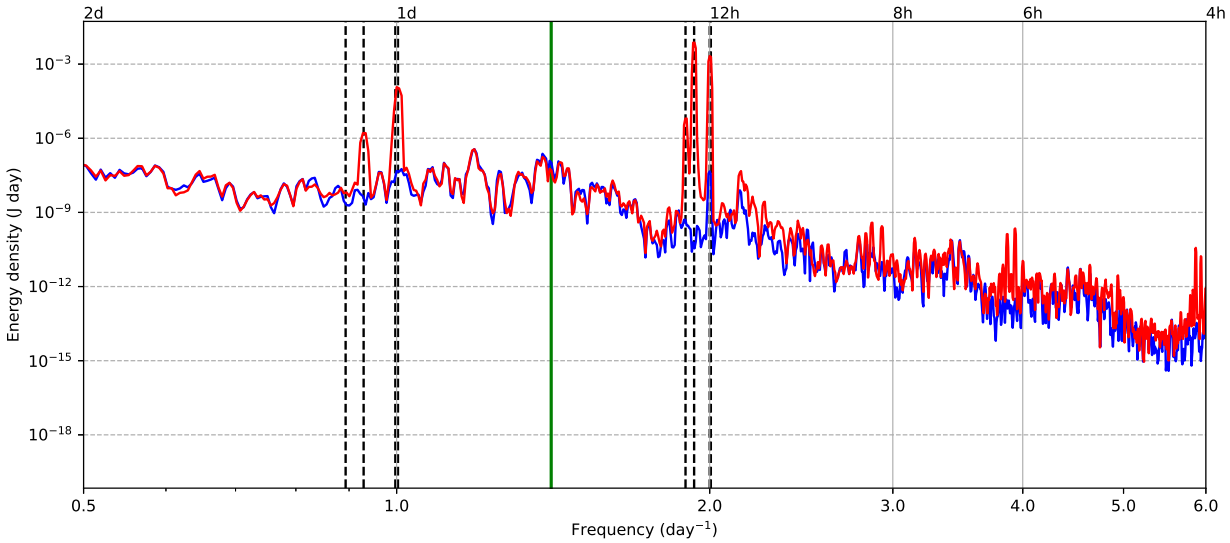

Figure S12: Barotropic rotary spectrum of kinetic energy density at the North Adriatic Sea point (44.77°N, 13.00°E), averaged across all depths, for a six-month period (January-June 2019). Dashed lines represent the eight tidal components included in the model, and the green line is the inertial frequency.

S3.5 Rhodes Gyre

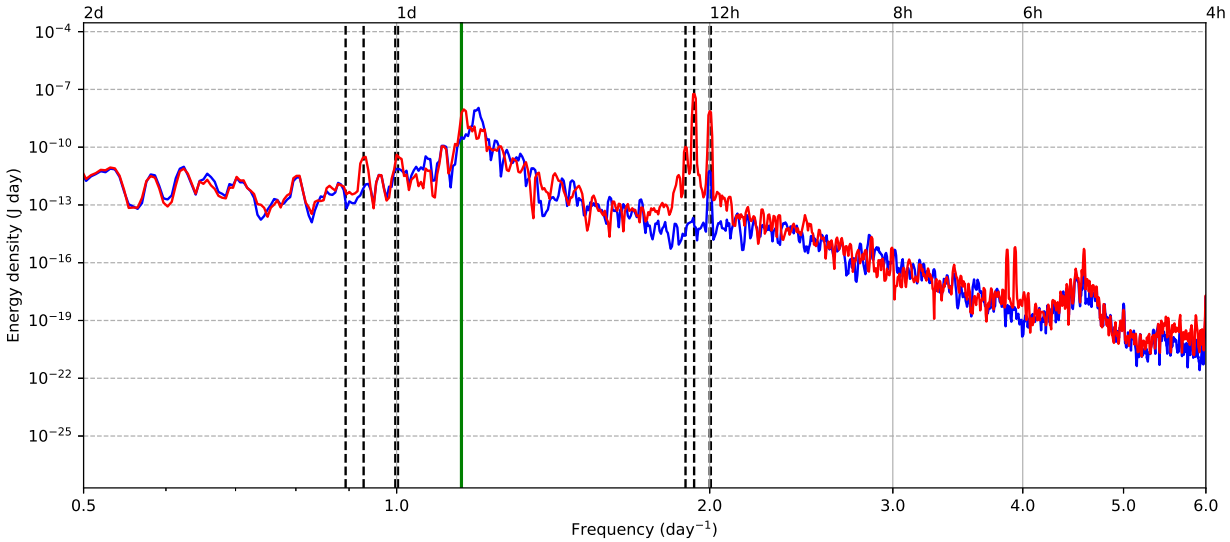

Figure S13: Barotropic rotary spectrum of kinetic energy density at the Rhodes Gyre point (35.27°N, 28.25°E), averaged across all depths, for a six-month period (January-June 2019). Dashed lines represent the eight tidal components included in the model, and the green line is the inertial frequency.

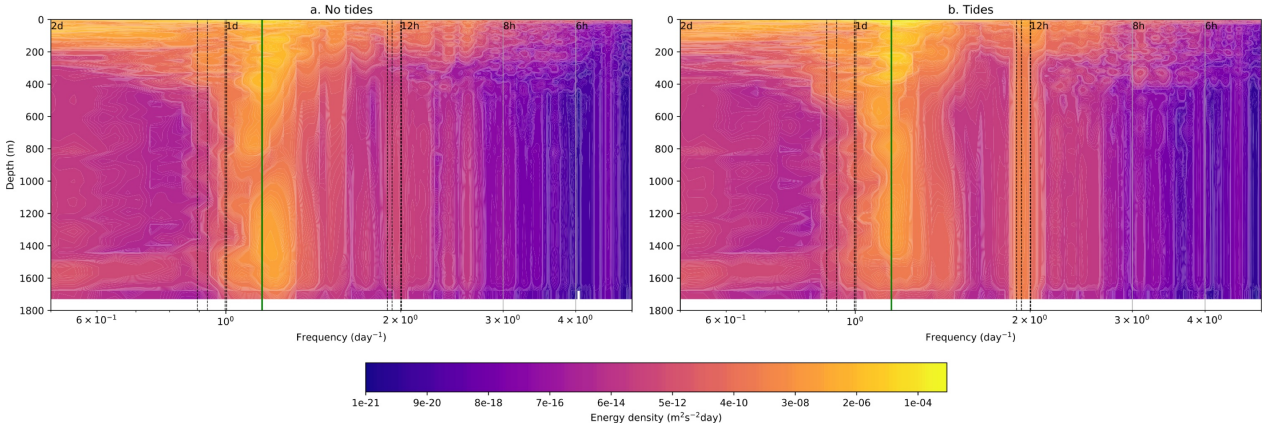

Figure S14: Rotary spectrum of kinetic energy density at the Rhodes Gyre point (35.27°N, 28.25°E), for all depths, over a six-month period (January-June 2019). Dashed lines represent the eight tidal components included in the model, and the green line is the inertial frequency.

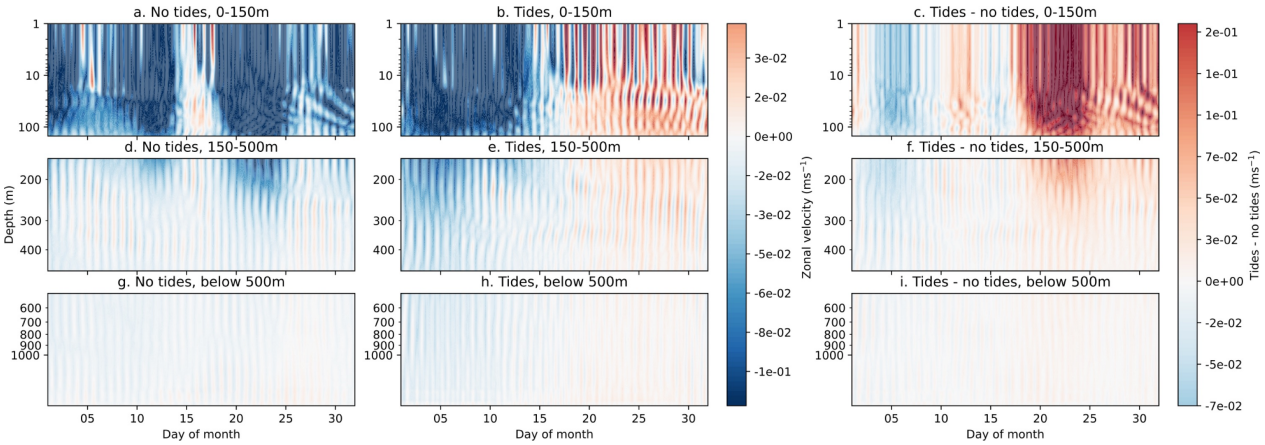

Figure S15: Hovmoller plots of depth against time of hourly mean zonal velocity at a point at the Rhodes Gyre point (35.27°N, 28.25°E) in May 2019, for a. Model without tides, 0-150m, b. Tidal model, 0-150m, c. Tidal model – model without tides, 0-150m, d. Model without tides, 150-500m, e. Tidal model, 150-500m, f. Tidal model – model without tides, g. Model without tides, below 500m, h. Tidal model, below 500m, i. Tidal model – model without tides, below 500m. Note that the depth scale is logarithmic.

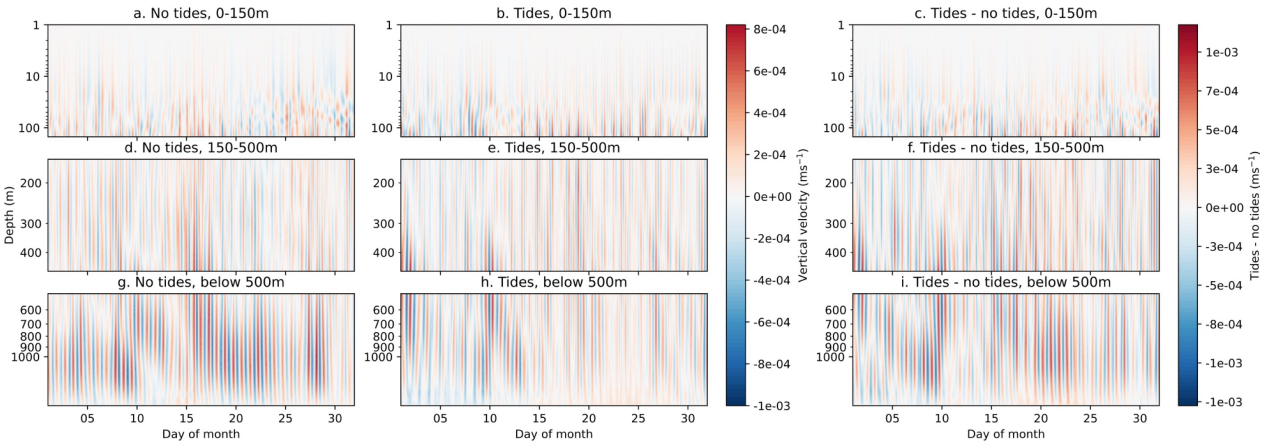

Figure S16: Hovmoller plots of depth against time of hourly mean vertical velocity at a point at the Rhodes Gyre point (35.27°N, 28.25°E) in May 2019, for a. Model without tides, 0-150m, b. Tidal model, 0-150m, c. Tidal model – model without tides, 0-150m, d. Model without tides, 150-500m, e. Tidal model, 150-500m, f. Tidal model – model without tides, g. Model without tides, below 500m, h. Tidal model, below 500m, i. Tidal model – model without tides, below 500m. Note that the depth scale is logarithmic.

S3.6 South Adriatic Sea

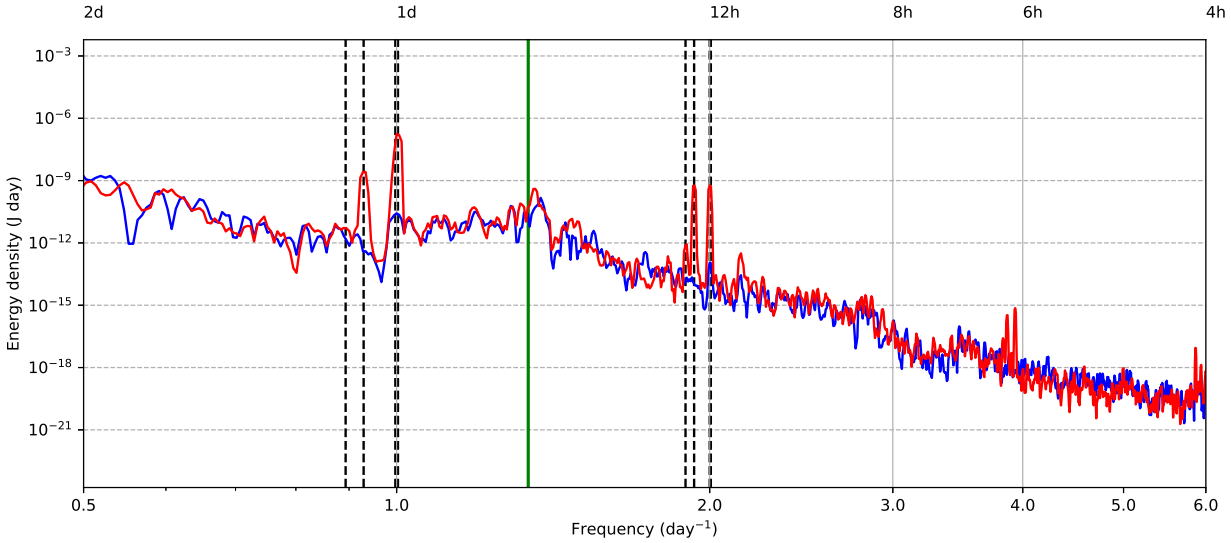

Figure S17: Barotropic rotary spectrum of kinetic energy density at the South Adriatic Sea point (42.02°N, 18.00°E), averaged across all depths, for a six-month period (January-June 2019). Dashed lines represent the eight tidal components included in the model, and the green line is the inertial frequency.

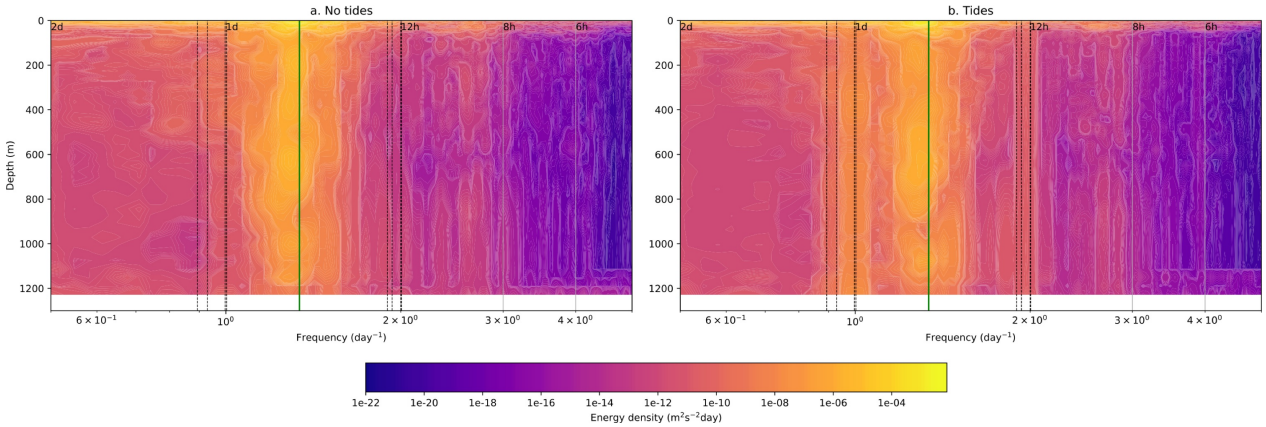

Figure S18: Rotary spectrum of kinetic energy density at the South Adriatic Sea point (42.02°N, 18.00°E), for all depths, over a six-month period (January-June 2019). Dashed lines represent the eight tidal components included in the model, and the green line is the inertial frequency.

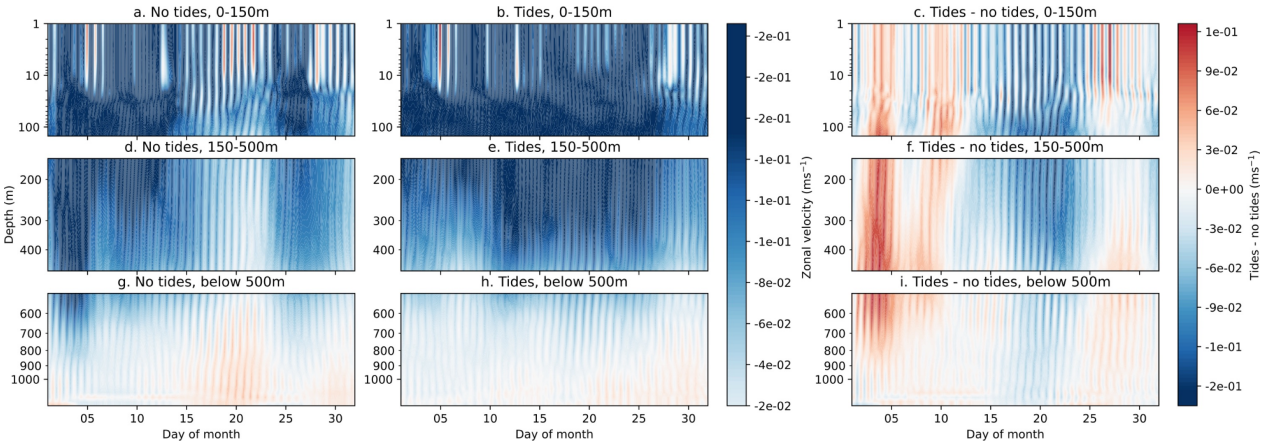

Figure S19: Hovmoller plots of depth against time of hourly mean zonal velocity at a point at the South Adriatic Sea point (42.02°N, 18.00°E) in May 2019, for a. Model without tides, 0-150m, b. Tidal model, 0-150m, c. Tidal model – model without tides, 0-150m, d. Model without tides, 150-500m, e. Tidal model, 150-500m, f. Tidal model – model without tides, g. Model without tides, below 500m, h. Tidal model, below 500m, i. Tidal model – model without tides, below 500m. Note that the depth scale is logarithmic.

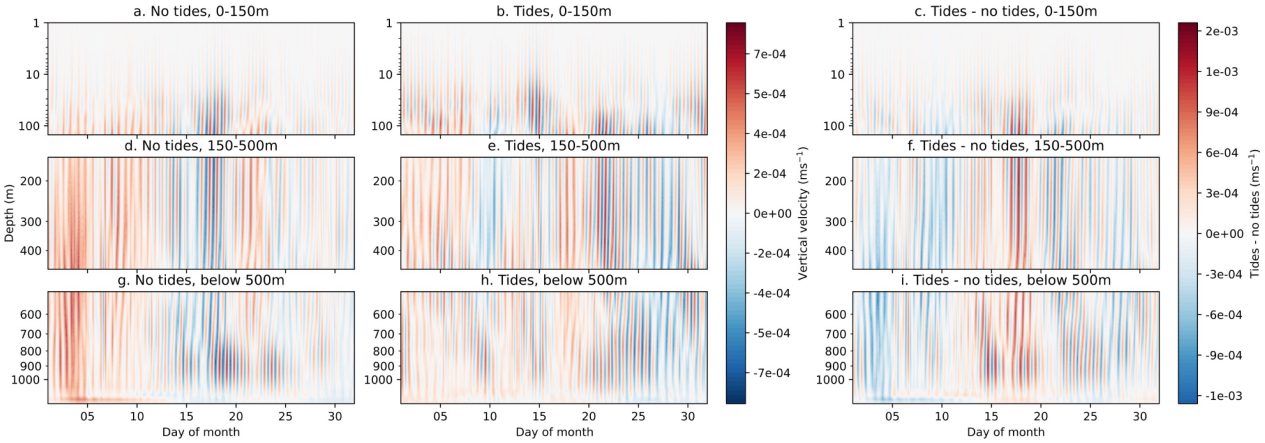

Figure S20: Hovmoller plots of depth against time of hourly mean vertical velocity at a point at the South Adriatic Sea point (42.02°N, 18.00°E) in May 2019, for a. Model without tides, 0-150m, b. Tidal model, 0-150m, c. Tidal model – model without tides, 0-150m, d. Model without tides, 150-500m, e. Tidal model, 150-500m, f. Tidal model – model without tides, g. Model without tides, below 500m, h. Tidal model, below 500m, i. Tidal model – model without tides, below 500m. Note that the depth scale is logarithmic.

References

Gonzalez, N. M., Waldman, R., Sannino, G., Giordani, H., and Somot, S.: Understanding tidal mixing at the Strait of Gibraltar: A high-resolution model approach, Progr. Oceanogr., 212, 102 980, https://doi.org/10.1016/j.pocean.2023.102980, 2023.

Harzallah, A., Alioua, M., and Li, L.: Mass exchange at the Strait of Gibraltar in response to tidal and lower frequency forcing as simulated by a Mediterranean Sea model, Tellus A: Dyn. Meteorol. Oceanogr., 66, 23 871, https://doi.org/10.3402/tellusa.v66.23871, 2014.

Naranjo, C., Lafuente, J., Sannino, G., and Sanchez-Garrido, J.: How much do tides affect the circulation of the Mediterranean Sea? From local processes in the Strait of Gibraltar to basin-scale effects, Progress Oceanogr., 127, 108–116, https://doi.org/j.pocean.2014.06.005, 2014.

Sannino, G., Herrmann, M., Carillo, A., Rupolo, V., Ruggiero, V., Artale, V., and Heimbach, P.: An eddy-permitting model of the Mediterranean Sea with a two-way grid refinement at the Strait of Gibraltar, Ocean Modell., 30, 56–72, https://doi.org//10.1016/j.ocemod.2009.06.002, 2009.

Soto-Navarro, J., Criado-Aldeanueva, F., García-Lafuente, J., and Sánchez-Román, A.: Estimation of the Atlantic inflow through the Strait of Gibraltar from climatological and in situ data, J. Geophys. Res. Oceans, 115, https://doi.org/10.1029/2010JC006302, 2010.